



HAL
open science

SOUND SYNTHESIS OF GONGS OBTAINED FROM NONLINEAR THIN PLATES VIBRATIONS: COMPARISON BETWEEN A MODAL APPROACH AND A FINITE DIFFERENCE SCHEME

Michele Ducceschi, Cyril Touzé, Stefan Bilbao

► **To cite this version:**

Michele Ducceschi, Cyril Touzé, Stefan Bilbao. SOUND SYNTHESIS OF GONGS OBTAINED FROM NONLINEAR THIN PLATES VIBRATIONS: COMPARISON BETWEEN A MODAL APPROACH AND A FINITE DIFFERENCE SCHEME. SMAC Stockholm Music Acoustics Conference 2013, Jul 2013, Stockholm, Sweden. hal-01138174

HAL Id: hal-01138174

<https://ensta-paris.hal.science/hal-01138174v1>

Submitted on 1 Apr 2015

HAL is a multi-disciplinary open access archive for the deposit and dissemination of scientific research documents, whether they are published or not. The documents may come from teaching and research institutions in France or abroad, or from public or private research centers.

L'archive ouverte pluridisciplinaire **HAL**, est destinée au dépôt et à la diffusion de documents scientifiques de niveau recherche, publiés ou non, émanant des établissements d'enseignement et de recherche français ou étrangers, des laboratoires publics ou privés.

SOUND SYNTHESIS OF GONGS OBTAINED FROM NONLINEAR THIN PLATES VIBRATIONS: COMPARISON BETWEEN A MODAL APPROACH AND A FINITE DIFFERENCE SCHEME.

Michele Ducceschi
UME - ENSTA Paristech
ducceschi@ensta.fr

Cyril Touzé
UME - ENSTA Paristech

Stefan Bilbao
University Of Edinburgh

ABSTRACT

The sound of a gong is simulated through the vibrations of thin elastic plates. The dynamical equations are necessarily nonlinear, crashing and shimmering being typical nonlinear effects. In this work two methods are used to simulate the nonlinear plates: a finite difference scheme and a modal approach. The striking force is approximated to the first order by a raised cosine of varying amplitude and contact duration acting on one point of the surface. It will be seen that for linear and moderately nonlinear vibrations the modal approach is particularly appealing as it allows the implementation of a rich damping mechanism by introducing a damping coefficient for each mode. In this way, the frequency-dependent decay rates can be tuned to get a very realistic sound. However, in many cases cymbal vibrations are found in strongly nonlinear regimes, where an energy cascade through lengthscales brings energy up to high-frequency modes. Hence, the number of modes retained in the truncation becomes a crucial parameter of the simulation. In this sense the finite difference scheme is usually better suited for reproducing crash and gong-like sounds, because this scheme retains all the modes up to (almost) Nyquist. However, the modal equations will be shown to have useful symmetry properties that can be used to speed up the off-line calculation process, leading to large memory and time savings and thus giving the possibility to simulate higher frequency ranges using modes.

1. INTRODUCTION

Thin plates are common mechanical elements found in several contexts in physics and engineering, from fluid-structure interaction, to aeronautics, civil engineering, wave turbulence [1–3], and others. The context of musical acoustics does not represent an exception, including linear and nonlinear examples. Plates are constitutive parts of several musical instruments: the soundboards of pianos and guitars are thin plates vibrating usually in a linear regime. Plates have been used in the past as reverberation units in music performances before the advent of digital software. Large

metallic plates were found at times in theatres as they can reproduce quite conveniently the sound of a storm when shaken.

When a thin plate is struck with a mallet or a hammer at large amplitudes, it produces a gong-like sound [4, 5]. Nonlinear effects caused by the large amplitudes of vibration are responsible for the crashing and shimmering sound similar to that of a gong [6]. These effects are reproduced by the von Kármán equations, who have proved to be an effective model for weakly nonlinear vibrations despite the introduction of a single second-order correction in the in-plane strain tensor with respect to the linear plate equations [7, 8].

Here the focus is on the resolution of the von Kármán equations in the context of sound synthesis obtained through physical modelling. A finite difference code developed by Bilbao [9, 10] is used as a benchmark for testing a code based on modal projection. The finite difference scheme is energy conserving and was used before in the analysis of thin plates in chaotic and turbulent regimes [1]. Although modal schemes have been employed several times in physical modelling of linear instruments, examples of their use for the production of sounds in a nonlinear context are rare. This is explained by the fact that the nonlinear modal equations can be quite involved, and therefore require a lot of memory and computational time, considering that the number of modes to be kept for synthesis is typically a few hundred.

In this work, some symmetries of the modal nonlinear plate equations are shown to help achieve memory and computational savings: in turn, this can help in the creation of faster synthesis algorithms. The most appealing feature of modal synthesis is the possibility of adding a rich damping mechanism with practically no extra effort: it is sufficient to add a damping term to each mode. The damping terms can be tuned at will, and they can be estimated in a real experiment, at least in a first approximation. In a finite difference code, on the contrary, damping can only be introduced in the time domain, thus limiting the implementation of a rich mechanism.

2. MODEL EQUATIONS

Consider a rectangular domain S of lengths L_x, L_y with boundary ∂S . Cartesian coordinates $\mathbf{x} \equiv (x, y)$ will be used to identify a point over S . Weakly nonlinear vibrations $w(\mathbf{x}, t)$ of the order of the plate thickness h are de-

scribed by the von Kármán equations. These are:

$$\rho h \ddot{w} = -D \Delta \Delta w - 2\sigma_0 \dot{w} + L(w, F) + P(\mathbf{x}, t); \quad (1a)$$

$$\Delta \Delta F = -\frac{Eh}{2} L(w, w). \quad (1b)$$

The function $F(\mathbf{x}, t)$ is an auxiliary function that describes the in-plane motion; it is usually referred to as Airy's stress function. The symbol Δ is the Laplacian; therefore in Cartesian coordinates $\Delta \Delta w \equiv (w_{,xx} + w_{,yy})^2$. $D = \frac{Eh^3}{12(1-\nu^2)}$ is the rigidity of the plate, where E is Young's modulus and ν is Poisson's ratio; ρ is the volume density. $P(\mathbf{x}, t)$ is a forcing term of some kind acting perpendicularly to the plate surface, and σ_0 is a damping coefficient. $L(\cdot, \cdot)$ is the nonlinear coupling term known as von Kármán operator, who reads:

$$L(w, F) = w_{,xx} F_{,yy} + w_{,yy} F_{,xx} - 2w_{,xy} F_{,xy}. \quad (2)$$

The system must be provided with boundary conditions along ∂S . In this work, simply supported boundary conditions with movable in-plane edges are chosen, *i.e.*

$$w = w_{,nn} = 0 \quad \forall \mathbf{x} \in \partial S, \quad (3a)$$

$$F = F_{,n} = 0 \quad \forall \mathbf{x} \in \partial S, \quad (3b)$$

where n is the direction normal to the boundary. These conditions describe edges fixed in the transverse direction, but free to rotate. In the in-plane direction the plate is free of loads.

2.1 Linear Modes and Modal Projection

A solution to system (1) can be obtained by projecting the functions w and F onto their linear modes. These are defined as:

$$w = S_w \sum_{i=1}^{N_w} \frac{\Phi_i(\mathbf{x})}{\|\Phi_i\|} q_i(t); \quad (4a)$$

$$\Delta \Delta \Phi_i(\mathbf{x}) = \frac{\rho h}{D} \omega_i^2 \Phi_i(\mathbf{x}). \quad (4b)$$

$$F = S_F \sum_{i=1}^{N_F} \frac{\Psi_i(\mathbf{x})}{\|\Psi_i\|} \eta_i(t); \quad (4c)$$

$$\Delta \Delta \Psi_i(\mathbf{x}) = \zeta_i^4 \Psi_i(\mathbf{x}). \quad (4d)$$

(4b) and (4d) are completed, respectively, by their boundary conditions (3a) and (3b). Note that N_w and N_F are, in theory, infinite. However they must be truncated to finite numbers for obvious computational reasons. As usual for linear problems, the modes are orthogonal with respect to a suitable scalar product. The scalar product between two modes Φ_i, Φ_j can be defined as

$$\langle \Phi_i, \Phi_j \rangle_S = \int_S d\mathbf{x} \Phi_i \Phi_j, \quad (5)$$

and the orthogonality condition imposes

$$\langle \Phi_i, \Phi_j \rangle_S = \|\Phi_i\|^2 \delta_{ij}, \quad (6)$$

with δ being Kronecker's delta. The norm of each mode is thus imposed by the scalar product. However, the constant S_w appearing in (4a) can be chosen so that the norm of the mode $S_w \Phi_i / \|\Phi_i\|$ becomes, precisely, S_w . The same is true for the modes Ψ_i and the constant S_F .

To obtain the modal equations, (4) is inserted into (1). Then one takes inner products of (1a) and (1b) with, respectively, $\Phi_s(\mathbf{x})$ and $\Psi_k(\mathbf{x})$ to get:

$$\begin{aligned} \ddot{q}_s + 2\chi_s \omega_s \dot{q}_s + \omega_s^2 q_s = \\ -\frac{ES_w^2}{2\rho} \sum_{n,p,q,r=1}^{\infty} \frac{H_{q,r}^n E_{p,n}^s}{\zeta_n^4} q_p q_q q_r + \frac{\langle \Phi_s, P(\mathbf{x}, t) \rangle_S}{\|\Phi_s\| \rho h S_w}. \end{aligned} \quad (7)$$

Note that the original σ_0 coefficient is replaced here by suitable χ_s coefficients, which are the modal damping coefficients. Regarding the forcing, one usually chooses a pointwise impulsion at the point \mathbf{x}_0 , therefore

$$P(\mathbf{x}, t) = \delta(\mathbf{x} - \mathbf{x}_0) p(t). \quad (8)$$

The form of $p(t)$ can be chosen as a raised cosine of the form

$$p(t) = \begin{cases} \frac{p_0}{2} (1 + \cos(\pi(t - t_0)/\Delta t)), & |t - t_0| \leq \Delta t \\ 0 & \text{otherwise.} \end{cases} \quad (9)$$

This creates a raised cosine of maximum amplitude p_0 centered around t_0 and of length Δt . This is a first approximation to a striking impulsion on the plate. Typically, for a timpani mallet one may choose $p_0 \approx 5 - 35$ N and $\Delta t \approx 5$ ms; for drum sticks $p_0 \approx 17 - 200$ N and $\Delta t \approx 0.15 - 0.3$ ms. Examples are given in fig. 1(a).

Note that, with the current choice for $P(\mathbf{x}, t)$ one gets

$$\langle \Phi_s, P(\mathbf{x}, t) \rangle_S = \Phi_s(\mathbf{x}_0) p(t). \quad (10)$$

Moreover, two third order tensors appear in (7). These are:

$$H_{q,r}^n = \frac{\langle \Psi_n, L(\Phi_q, \Phi_r) \rangle_S}{\|\Psi_n\| \|\Phi_q\| \|\Phi_r\|}; \quad (11a)$$

$$E_{p,n}^s = \frac{\langle \Phi_s, L(\Phi_p, \Psi_n) \rangle_S}{\|\Phi_p\| \|\Phi_s\| \|\Psi_n\|}. \quad (11b)$$

The two tensors can be combined to give

$$\Gamma_{p,r,q}^s \equiv \sum_{n=1}^{N_F} \frac{H_{q,r}^n E_{p,n}^s}{\zeta_n^4}; \quad (12)$$

this tensor is the tensor of coupling coefficients for the modal equations. It is fourth order because the modal equations are cubic with respect to the modal coordinates $q_s(t)$.

2.1.1 Solutions to The Eigenvalue Problems

A solution to (4b) with boundary conditions (3a) is obtained immediately by considering

$$\Phi_i(\mathbf{x}) = \sin\left(\frac{i_1 \pi x}{L_x}\right) \sin\left(\frac{i_2 \pi y}{L_y}\right), \quad (13)$$

for integers i_1, i_2 . This gives the following eigenfrequencies of vibration:

$$\omega_i^2 = \frac{D}{\rho h} \left[\left(\frac{i_1 \pi}{L_x}\right)^2 + \left(\frac{i_2 \pi}{L_y}\right)^2 \right]^2. \quad (14)$$

On the other hand, for the Airy stress function modes there is no analytical solution. It is worth noticing that the eigenvalue problem (4d) with boundary conditions (3b) corresponds mathematically to the problem of a clamped Kirchhoff plate, even though it describes the physical situation of in-plane motion free of loads at the boundary. The question is then how to find the modes of a Kirchhoff plate with clamped edges. A possible strategy is to construct an appropriate algebraic eigenvalue problem starting from energy considerations. This is known as Galerkin's method. This method is based on the assumption that the generic eigenfunction Ψ_k can be written as a weighted sum of chosen expansion functions, hence:

$$\Psi_k(\mathbf{x}) = \sum_{n=1}^{N_c} a_k^n \Lambda_n(\mathbf{x}). \quad (15)$$

The rate of convergence and accuracy of such a method relies heavily on the expansion functions used to approximate the sought solution, as well as on the total number of functions, N_c . Obviously the expansion functions must form a complete set over the domain of interest; in addition they need to satisfy all the geometric boundary conditions. The case of the clamped plate presents two such conditions, namely zero displacement and zero slope at the boundary. Usually one resorts to modification of Fourier series, for which completeness follows directly from the Fourier theorem. In addition, satisfaction of the boundary conditions can be achieved by adding a fourth order polynomial to the Fourier series, as explained in [11]. Hence for the clamped plate problem one may use

$$\Lambda_n(\mathbf{x}) = X_{n_1}(x)Y_{n_2}(y), \quad (16)$$

where

$$X_{n_1}(x) = \cos\left(\frac{n_1\pi x}{L_x}\right) + \frac{15(1 + (-1)^{n_1})}{L_x^4}x^4 - \frac{4(8 + 7(-1)^{n_1})}{L_x^3}x^3 + \frac{6(3 + 2(-1)^{n_1})}{L_x^2}x^2 - 1, \quad (17)$$

and similarly for $Y_{n_2}(y)$. The eigenvalue problem may be written in the form

$$K\mathbf{a} = \zeta^4 M\mathbf{a}; \quad (18)$$

this gives the expansion coefficients a_k^n along with the eigenvalues ζ_k . The stiffness and mass matrices are obtained from energy considerations [11], and they read:

$$K_{ij} = \langle \Delta \Lambda_i, \Delta \Lambda_j \rangle_S - \int_S d\mathbf{x} L(\Lambda_i, \Lambda_j), \quad (19a)$$

$$M_{ij} = \langle \Lambda_i, \Lambda_j \rangle_S. \quad (19b)$$

2.2 The Finite Difference Approximation

Time and space are discretised so that the continuous variables (x, y, t) are approximated by their discrete counterparts (lh_x, mh_y, nh_t) , where (l, m, n) are integer indices and (h_x, h_y, h_t) are the steps. Boundedness of the domain implies that $(l, m) \in [0, N_x] \times [0, N_y]$ so that the grid size

is given by $(N_x + 1) \times (N_y + 1)$. The continuous variables $w(\mathbf{x}, t)$, $F(\mathbf{x}, t)$ are then approximated by $w_{l,m}^n$, $F_{l,m}^n$ at the discrete time n for the grid point (l, m) . Time shifting operators are introduced as

$$e_{t+} w_{l,m}^n = w_{l,m}^{n+1}, \quad e_{t-} w_{l,m}^n = w_{l,m}^{n-1}. \quad (20)$$

Time derivatives can then be approximated by:

$$\delta_t = \frac{1}{2h_t}(e_{t+} - e_{t-}), \quad \delta_{t+} = \frac{1}{h_t}(e_{t+} - 1),$$

$$\delta_{t-} = \frac{1}{h_t}(1 - e_{t-}), \quad \delta_{tt} = \delta_{t+}\delta_{t-}. \quad (21)$$

Time averaging operators are introduced as:

$$\mu_{t+} = \frac{1}{2}(e_{t+} + 1), \quad \mu_{t-} = \frac{1}{2}(1 + e_{t-}),$$

$$\mu_t = \frac{1}{2}(e_{t+} + e_{t-}), \quad \mu_{tt} = \mu_{t+}\mu_{t-}. \quad (22)$$

Similar definitions hold for the space operators. Hence, the Laplacian Δ and the double Laplacian $\Delta\Delta$ are given by:

$$\delta_\Delta = \delta_{xx} + \delta_{yy}, \quad \delta_{\Delta\Delta} = \delta_\Delta \delta_\Delta. \quad (23)$$

The von Kármán operator at interior points $L(w, F)$ can then be discretised as:

$$l(w, F) = \delta_{xx}w\delta_{yy}F + \delta_{yy}w\delta_{xx}F - 2\mu_x\mu_y(\delta_{x+y}w\delta_{x+y}F). \quad (24)$$

Thus the discrete counterpart of (1) is:

$$D\delta_{\Delta\Delta}w + \rho h\delta_{tt}w = l(w, \mu_t F) - 2\sigma_0\delta_t w + P_{l,m}^n; \quad (25a)$$

$$\mu_{t-}D\delta_{\Delta\Delta}F = -\frac{Eh}{2}l(w, e_{t-}w). \quad (25b)$$

Such a scheme is energy conserving, where the discrete energy is positive definite and yields a stability condition, as proved in [9, 10]. Implementation of boundary conditions is explained thoroughly in [10]. For the sound synthesis of a struck plate, however, the constraint of energy conservation may be relaxed: if the initial amplitude of vibration is not too large (typically less than $10\sqrt{L_x L_y}$), the damping effects will make sure that the time series will not become unstable. A faster scheme than can then be implemented, and this is:

$$D\delta_{\Delta\Delta}w + \rho h\delta_{tt}w = l(w, F) - 2\sigma_0\delta_t w + P_{l,m}^n; \quad (26a)$$

$$D\delta_{\Delta\Delta}F = -\frac{Eh}{2}l(w, w). \quad (26b)$$

2.3 Convergence of Γ coefficients

Table 1 presents a convergence test of the Γ tensor for a plate of aspect ratio $\xi = L_x/L_y = 2/3$. The convergence in this case depends on two factors: the first is the amount of stress function modes retained in the definition of Γ (N_F in eq. (12)); the second is the accuracy on the Airy stress function modes and frequencies (quantified by the number N_c in eq. (15)). For clarity, in the following tables

| | | N_F | | |
|------------|--|---------------------|---------------------|---------------------|
| k | | 100 | 144 | 225 |
| 1 | | 20.033 | 20.034 | 20.034 |
| 20 | | $7.5605 \cdot 10^3$ | $9.4893 \cdot 10^3$ | $9.4960 \cdot 10^3$ |
| 50 | | $1.3928 \cdot 10^4$ | $1.3929 \cdot 10^4$ | $1.3937 \cdot 10^4$ |
| 100 | | $1.4847 \cdot 10^4$ | $2.7360 \cdot 10^4$ | $1.2413 \cdot 10^5$ |
| | | 400 | 484 | 625 |
| 1 | | 20.034 | 20.034 | 20.034 |
| 20 | | $9.4970 \cdot 10^3$ | $9.4975 \cdot 10^3$ | $9.4977 \cdot 10^3$ |
| 50 | | $1.3937 \cdot 10^4$ | $1.3937 \cdot 10^4$ | $1.3937 \cdot 10^4$ |
| 100 | | $1.3334 \cdot 10^5$ | $2.2100 \cdot 10^5$ | $2.2108 \cdot 10^5$ |

Table 1. Convergence of coupling coefficients, $\Gamma_{k,k,k}^k (L_x L_y)^3$, $\xi = 2/3$.

| | | Grid Points | | |
|------------|--|---------------------|---------------------|---------------------|
| k | | 51×76 | 161×241 | 280×419 |
| 1 | | 20.728 | 20.381 | 20.189 |
| 20 | | $9.7935 \cdot 10^3$ | $9.6413 \cdot 10^3$ | $9.5567 \cdot 10^3$ |
| 50 | | $1.4440 \cdot 10^4$ | $1.4234 \cdot 10^4$ | $1.4080 \cdot 10^4$ |
| 100 | | $2.0223 \cdot 10^5$ | $2.0246 \cdot 10^5$ | $2.0286 \cdot 10^5$ |

Table 2. Convergence of coupling coefficients, FD scheme, $\Gamma_{k,k,k}^k (L_x L_y)^3$, $\xi = 2/3$, $N_F = 225$

N_F is always the same as N_c . It is seen that a four-digit convergence up to the $\Gamma_{100,100,100}^{100}$ coefficient is obtained when $N_F = 484$. The same coefficients can be calculated using the finite difference code. Results are summarised in table 2. It is seen that the coupling coefficients can be calculated to very high precision when using the modal description. The major drawback of the modal approach is the limited number of modes that one can keep for the simulations (≈ 200). On the other hand, the finite difference scheme produces simulations including a vast number of modes (≈ 10000), at the expense of numerical precision. Comparing tables 1 and 2 suggests that a four-digit convergence is out of reach for the finite difference scheme with typical grid sizes. The question is then which one of the two methods is better suited for sound synthesis.

3. EXAMPLE: A STRUCK PLATE

In this section an example is investigated to compare the two methods. The reference plate is a steel plate of dimensions $L_x \times L_y = 0.4 \times 0.6$ m², Young's modulus $E = 2 \cdot 10^{11}$ Pa, density $\rho = 7860$ kg/m³, Poisson's ratio $\nu = 0.3$ and thickness $h = 1$ mm. The plate is excited with a temporal raised cosine at one point, with $\Delta t = 0.1$ ms and varying amplitude p_0 . The damping factor is $\omega_s \chi_s = 0.75$ s⁻¹, resulting in $\sigma_0 = 0.75 \rho h$ kg/m².

The finite difference scheme is run at 100 kHz, resulting in a grid size of 51×76 points. Scheme (25) takes about two hours of calculation per second of simulation, on a machine running MATLAB equipped with Intel Core i5 CPU 650 @ 3.20GHz. However, the simpler scheme (26)

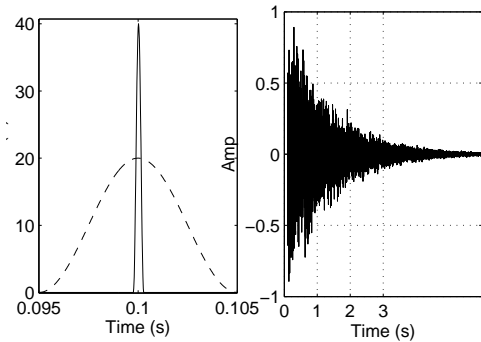


Figure 1. (a) Raised cosine simulating the impacts of a timpani mallet (dashed line) and a wooden drumstick (solid line). (b) Normalised time series obtained from the modal scheme when the plate is excited with a raised cosine of amplitude 15 N and $\Delta t = 0.1$ ms, and having a damping factor $\sigma_0 = 0.75 \rho h$ kg/m².

is faster and requires about an hour of calculation for the same simulation parameters.

On the other hand, for the modal approach the biggest issue results in the calculation of the Γ tensor. However, this calculation is performed off-line once and for all. It is worth noticing that the same tensor can be used for all problems sharing the same boundary conditions and aspect ratio. The typical maximum size achievable for a fourth order tensor of dimension N_w^4 is reached when N_w (the total number of displacement modes) is about 150; in this case the tensor occupies about 1 GB of memory. From section 2.3 it is seen that a reasonable convergence of the Γ tensor is obtained when $N_F = 484$. The calculation of Γ with $N_F = 484$, $N_w = 150$ takes about 0.5 hours in MATLAB. Once the tensor is ready, one can design a basic Störmer-Verlet scheme for the time integration [12]. This is achieved by replacing $\frac{d^2}{dt^2}$, $\frac{d}{dt}$ with their discrete counterparts δ_{tt} , δ_t in (7). For sound synthesis, this scheme can be run at lower sampling rates, typically 20kHz; doing so results in a calculation time of about 10 minutes per second of simulation. The time series produced by the modal scheme for $p_0 = 15$ N is shown in fig.1(b). Although the envelope resembles that of a decaying impulsion, the high frequency content of the time series is really poor: this is where the truncation to $N_w = 150$ modes rears its head. Fig.2 compares the spectrograms obtained from finite differences and modes, in the case of three forcing cases: $p_0 = 15, 100, 200$ N (top to bottom). As the excitation grows, energy is passed to higher parts of the spectrum, which bear significant perceptual information. The flow of energy towards smaller scales should be interpreted in the realm of wave turbulence [2]; in actual fact, wave turbulence in vibrating plates is the subject of extensive studies [1,3,8]. A turbulent flow is characterised by the flow of energy to higher frequencies up to the dissipation scales; however the modal truncation does not allow the energy to flow past 5000 Hz, a limit which makes the plate sound dull

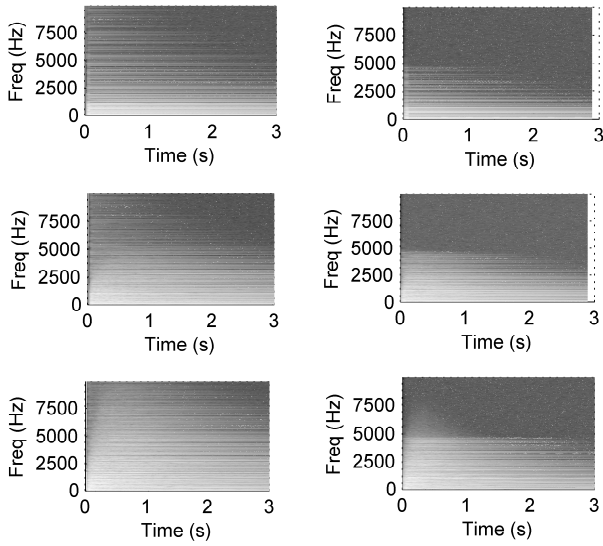


Figure 2. Comparison between FD (left) and modes (right) for $p_0 = 15$ N (top), 100 N (middle), 200 N (bottom). The modal truncation at $N_w = 150$ modes is evident in all cases.

and colourless. The finite difference scheme, on the contrary, produces a much brighter and sharp sound, because the frequency spectrum is much larger (for a sampling rate of 100kHz, the upper limit is about 40kHz). The question is then how to spare memory space in the calculation of the Γ tensor, and possibly how to speed up its calculation. This is the subject of the next section.

4. CALCULATION SHORTCUTS

4.1 Symmetry Properties

Useful symmetries can be derived for the Γ tensor. A first obvious property is the following:

$$H_{p,q}^i = H_{q,p}^i. \quad (27)$$

This follows directly from the definition of $L(\cdot, \cdot)$, which is bilinear in its entries. A second, less straightforward property is obtained when integrating by parts the tensor E from (11b). This gives

$$E_{p,q}^n = H_{p,n}^q + \oint \mathbf{n} \cdot \delta \mathbf{S} G_{p,q}^n \quad (28)$$

where G is a third order tensor depending on Ψ_n , Φ_p , Φ_q and their derivatives along the boundary. It was noted in [7] that the selected boundary conditions make the integral vanish. In this way, the tensor Γ may then be conveniently written as

$$\Gamma_{p,q,r}^s = \sum_{n=1}^{N_F} \frac{H_{p,q}^n H_{r,s}^n}{\zeta_n^4}. \quad (29)$$

Basically the symmetry properties for Γ mean the following sets of indices will produce the same numerical value:

$$(s, p, q, r), (r, p, q, s), (s, q, p, r), (r, q, p, s),$$

$$(q, r, s, p), (p, r, s, q), (q, s, r, p), (p, s, r, q).$$

These symmetry properties can lead to large memory savings when the number of transverse and in-plane modes is a few hundred.

4.2 Null Coupling Coefficients

For the sake of numerical computation, it would be interesting to know *a priori* which coupling coefficients are null. In actual fact, empirical observations of the Γ tensor suggest that only a smaller fraction of coefficients is not zero. As an example, consider fig.3. In this figure some of the coefficients $\Gamma_{p,q,r}^n$ are plotted for given n, p and for $q = r = 1 : 10$. A black slot corresponds to a value of zero. It is clear that more than half of the coefficients is vanishing. Thus, an *a priori* knowledge of their occurrences could lead to huge memory and computational savings. Referring to fig.3, one may notice that the patterns depicted in the diagrams of the left column are repeated exactly by the adjacent diagrams in the right column. This suggests that the modes can be grouped in families whose members share the same coupling rules with respect to members of another family. A straightforward way to divide the modes on the plate is to consider the symmetry of their shape with respect to a coordinate system with origin at the centre of the plate. Four families exist, and these are: doubly symmetric (SS), antisymmetric-symmetric (AS and SA) and doubly antisymmetric (AA). For instance, the first mode is a doubly-symmetric mode because it presents one maximum at the centre of the plate, and is thus symmetric with respect to the two orthogonal directions departing from the centre of the plate in the x and y directions. The first few modes for the case under study may be classified in the following groups:

- SS: 1,4,8,11,12,20,...
- SA: 2,7,9,14,16,...
- AS: 3,6,13,15,19,...
- AA: 5,10,17,18,...

Observing the black slots of fig.3 permits to state the following heuristic rule:

the indices (s, p, q, r) will give a nonzero value for $\Gamma_{p,q,r}^s$ if and only if modes s,p,q,r come all from distinct modal shape groups or if they come from the same group two by two.

For example, the combinations (SS, SS, AS, SA) and (SS, SS, SS, AS) will definitely give a zero value; on the other hand the combinations (SS, SS, SS, SS), (SS, AA, SS, AA) and (SS, AS, SA, AA) will give a nonzero value. A rigorous mathematical proof is not carried out as it involves a rather lengthy development which is beyond the scope of the present work. For the sake of generality, it should be mentioned that similar symmetries hold for other boundary conditions in rectangular and circular geometries [7, 13]. Thanks to this interpretation it is easy to see why the left column diagrams are reproduced symmetrically in the right

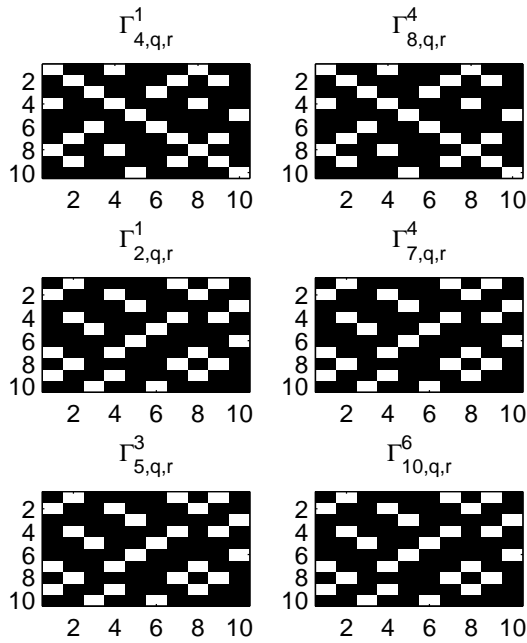


Figure 3. The null coupling coefficients (black squares) are placed in the slots predicted by the heuristic rule.

column: the modes chosen for the two columns come from the same families, hence they give rise to the same zero coefficients. This rule, in combination with the previous remarks on symmetry, can be used to speed up the calculation of the Γ tensor (for example by pre-allocating the zero entries when using a sparse matrix description). Ideally, a tensor comprising 400 - 500 modes should be used for sound synthesis, in order to be able to simulate frequencies up to 10kHz.

5. CONCLUSIONS

This work presented a comparison between a finite difference and a modal scheme for the reproduction of the nonlinear vibrations of a thin, metallic plate, aiming at simulating the sound emitted by a gong struck by an impulsive force (like a mallet). The two methods were shown to yield the same results, within the bounds imposed by numerical approximation. The problems induced by modal truncation were highlighted and their influence on the sound produced described. It was seen that symmetry and coupling rules are desirable to the extent of reducing the burden deriving from the calculation of the coupling coefficient tensor. These properties were shown, leading to an a priori knowledge of the null coupling coefficients. These coefficients constitute more than a half of the total coefficients. This work opens the possibility to construct a very effective and precise modal scheme for nonlinear vibrations: the coupling coefficients can be calculated to very high precision, and a fine damping mechanism can be implemented in the modal equations. Sound samples from the finite difference and modal schemes will be played at the conference, for

both rectangular and circular geometries.

6. REFERENCES

- [1] C. Touzé, S. Bilbao, and O. Cadot, “Transition scenario to turbulence in thin vibrating plates,” *Journal of Sound and Vibration*, vol. 331, no. 2, pp. 412–433, 2011.
- [2] G. Düring, C. Josserand, and S. Rica, “Weak turbulence for a vibrating plate: Can one hear a kolmogorov spectrum?” *Phys. Rev. Lett.*, vol. 97, p. 025503, 2006.
- [3] A. Boudaoud, O. Cadot, B. Odille, and C. Touzé, “Observation of wave turbulence in vibrating plates,” *Phys. Rev. Lett.*, vol. 100, p. 234504, 2008.
- [4] C. Touzé, S. Bilbao, L. Longo-Mucciante, O. Cadot, and A. Boudaoud, “Vibrations chaotiques de plaques minces: application aux instruments de type cymbale,” in *Proceedings of CFA 2010, 10eme Congrès Français d’Acoustique*, Lyon, April 2010.
- [5] K. A. Legge and N. H. Fletcher, “Nonlinearity, chaos, and the sound of shallow gongs,” *The Journal of the Acoustical Society of America*, vol. 86, no. 6, pp. 2439–2443, 1989.
- [6] A. Chaigne, C. Touzé, and O. Thomas, “Nonlinear vibrations and chaos in gongs and cymbals,” *Acoustical Science and Technology*, vol. 26, pp. 403–409, 2005.
- [7] O. Thomas and S. Bilbao, “Geometrically nonlinear flexural vibrations of plates: In-plane boundary conditions and some symmetry properties,” *Journal of Sound and Vibration*, vol. 315, no. 3, pp. 569–590, 2008.
- [8] C. Touzé, O. Thomas, and M. Amabili, “Transition to chaotic vibrations for harmonically forced perfect and imperfect circular plates,” *International Journal of Non-Linear Mechanics*, vol. 46, no. 1, pp. 234 – 246, 2011.
- [9] S. Bilbao, “A family of conservative finite difference schemes for the dynamical von Kármán plate equations,” *Numerical Methods for Partial Differential equations*, vol. 24, no. 1, pp. 193–216, 2008.
- [10] —, *Numerical Sound Synthesis: Finite Difference Schemes and Simulation in Musical Acoustics*. Wiley, 2009.
- [11] W. Li, “Vibration analysis of rectangular plates with general elastic support,” *Journal of Sound and Vibration*, vol. 273, no. 3, pp. 619–635, 2003.
- [12] E. Hairer, C. Lubich, and G. Wanner, *Geometric Numerical Integration*. Springer, 2006.
- [13] O. Thomas, C. Touzé, and A. Chaigne, “Non-linear vibrations of free-edge thin spherical shells: modal interaction rules and 1:1:2 internal resonance,” *International Journal of Solids and Structures*, vol. 42, no. 1112, pp. 3339 – 3373, 2005.